

Molecular Transformation of Crude Oil Contaminated Soil after Bioelectrochemical Degradation Revealed by FT-ICR Mass Spectrometry

Huan Wang, Lu Lu, Huan Chen, Amy M. McKenna, Jie Lu, Song Jin, Yi Zuo, Fernando L. Rosario-Ortiz, and Zhiyong Jason Ren*

Cite This: *Environ. Sci. Technol.* 2020, 54, 2500–2509

Read Online

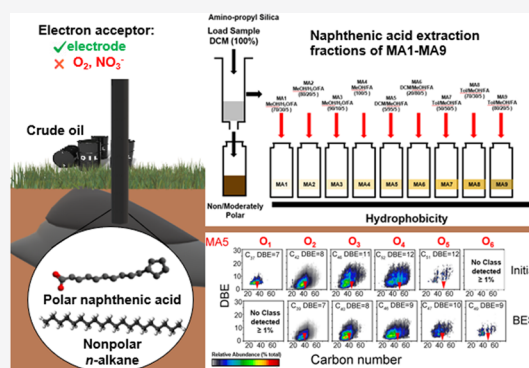
ACCESS |

Metrics & More

Article Recommendations

Supporting Information

ABSTRACT: Bioremediation is a low-cost approach for crude oil spill remediation, but it is often limited by electron acceptor availability. In addition, the biodegradation products of crude oil contaminants are complex, and transformation pathways are difficult to decipher. This study demonstrates that bioelectrochemical systems (BESs) can be effective in crude oil degradation by integrating biological and electrochemical pathways, and more importantly, it provides the first understanding on the daughter products of bioelectrochemical hydrocarbon degradation. Using electrospray ionization (ESI) Fourier transform ion cyclotron resonance mass spectrometry (FT-ICR MS) and two-dimensional gas chromatography (GC × GC), the results showed that the active BES reactor improved the total petroleum hydrocarbon (TPH) degradation by ~70% than open circuit control reactors. After separating the daughter products into nine fractions (MA1–MA9) according to the molecular weight (m/z 200–1000) by modified amino-propyl silica (MAPS) fractionation, we found that active BES remediation resulted in 50% more polar, oxygen-containing naphthenic (NAP) acids. The MA4 fraction (centered at ~550 Da) increased by 47%, and MA5 and MA7 fractions with higher molecular weight increased by a maximum of ~7- and 9-fold, respectively. These results are in accordance with the variation of bulk elemental compositions in O_2 species, where daughter transformation products doubled relative to parent oil extract. The contribution of newly generated NAP acids was mainly from higher-order oxygen species (O_5 – O_6) with increased hydrophobicity in conjunction with a decreased abundance in lower-order oxygen species (O_1). Overall, the study suggests that n -alkane degradation occurred via β -oxidation to oxygenated transformation products with lower molecular weight, such as n -alcohols in O_1 class and subsequently to n -fatty acids in O_2 class.



INTRODUCTION

Crude oil spills are among the most disastrous environmental problems due to the recalcitrant and complex nature of the contaminants. Crude oil is a highly heterogeneous mixture that consists of ~85–90% CH (hydrocarbons) and ~10–15% polar heteroatom NSO (nitrogen, sulfur, or oxygen) species.¹ These petroleum hydrocarbons can be degraded biologically following multiple biochemical pathways (e.g., oxidation, reduction, hydroxylation, and dehydrogenation), but the degradation rate largely depends on the availability of electron acceptors (e.g., oxygen, nitrate, iron, sulfate, etc.).^{2–4} The susceptibility of different hydrocarbons to microbial attack can vary significantly. In general, n -alkanes are the least recalcitrant and most susceptible compounds, followed by branched alkanes, monocyclic saturated and monoaromatic hydrocarbons, polynuclear aromatic hydrocarbons, and heteroatomic species.⁵ Biodegradation can be confirmed by decreasing in relative abundance of saturated and aromatic hydrocarbons as well as an increase of polar fractions.⁶ However, newly

generated polar oxygenated daughter products including naphthenic (NAP) acids⁷ may be more resistant to microbial catabolism⁸ and even more toxic compared to their parent contaminants.⁹ Therefore, it is critical to understand the compositional changes during degradation.

Because nontargeted oxygenation products are not amenable to gas or liquid chromatographic analysis due to high polarity and low volatility,¹⁰ Fourier transform ion cyclotron resonance mass spectrometry (FT-ICR MS) has been employed to obtain ultrahigh resolving power, routinely resolving 26,000 mass spectral peaks separated with carbon atoms up to C_{100} for n -alkanes,¹¹ making it possible to separate and identify highly polar, oxygen-containing compounds at molecular levels.¹⁰

Received: October 12, 2019

Revised: January 19, 2020

Accepted: January 27, 2020

Published: January 27, 2020

Coupled with electrospray ionization (ESI), which can achieve selective ionization of polar compounds,⁷ FT-ICR MS has been successfully applied to characterize the polar compounds generated from aerobic or anaerobic biodegradation of crude oil.^{8,12}

Natural attenuation-based *in situ* bioremediation is cost-effective and less intrusive compared to physical or chemical processes,¹³ but it is slow, and the degradation products are complex.^{14,15} Recently, the bioelectrochemical remediation method was developed and tested to accelerate hydrocarbon biodegradation in the laboratory, and pilot scale studies have been conducted in groundwater,¹⁶ sediments,¹⁷ and soil¹⁸ with promising results. Bioelectrochemical systems (BESs) integrate biological and electrochemical processes by employing electroactive bacteria (EAB) and their syntrophic partners to oxidize petroleum hydrocarbons and respire the anode as the electron acceptor.¹⁹ The electrons harvested from the anode are transferred through an external circuit to the cathode, where terminal electron acceptors (e.g., oxygen) are reduced.²⁰ Bioelectrochemical remediation offers a number of advantages including passive remediation without disturbing the soil matrix, increasing degradation rate via electrochemically boosted biodegradation, and nonintrusive online monitoring. The remediation process is energy-positive by producing current, which can even provide energy for remote sensors.^{21–23}

Many previous BES studies target specific pollutants, such as toluene or benzene,^{24,25} so the degradation can be characterized by gas chromatography (GC). For those studies using actual hydrocarbon contaminated soil, the characterization was limited to the overall measurement of total petroleum hydrocarbon (TPH) and polycyclic aromatic hydrocarbons (PAH) by GC-FID or GC-MS.^{18,23,26} Such data provide general information on hydrocarbon removal, lacking detailed insights on degradation mechanisms and products characterization.

In this study, we investigated how bioelectrochemical remediation could enhance crude oil biodegradation. More importantly, we first investigate the bioelectrochemical degradation products by employing GC, GC × GC MS, as well as (–) ESI coupled with FT-ICR MS. We reported the reactor performance, which proved the enhancement of BES for crude oil degradation. We also explored the biodegradation mechanisms of nonpolar hydrocarbon compounds and molecular-level compositional variations on polar (acidic), oxygen-containing transformation products.

MATERIALS AND METHODS

Soil Collection and Characterization. Crude oil-contaminated soil (total petroleum hydrocarbon (TPH) concentration of 24,085 mg/kg-dry-soil) collected from polluted sites in Michigan, US, was provided by the Chevron Energy Technology Company. Before being used in the experiment, the soil was saturated with artificial groundwater (4 mM Na⁺, 0.2 mM Ca²⁺, 0.1 mM Mg²⁺, 2.4 mM Cl[–], 2 mM HCO₃[–], and 0.1 mM SO₄^{2–} in deionized water, conductivity ≈ 0.05 S/m at 22 °C, pH ≈ 8.2), and no additional buffer was added to amend conductivity and pH. The main characteristics of the initial soil were summarized in Table S1.

Soil BES Configuration and Operation. Experiments were carried out in bottle-type dual-chamber BES reactors (300 mL volume for each chamber, Figure S1). Anode and cathode chambers that were separated by a cation exchange

membrane were filled with 250 mL saturated soil and artificial groundwater, respectively, which were purged with ultra-high-purity nitrogen gas to remove dissolved oxygen before being added to the reactor. The anode and cathode were a carbon fiber brush (diameter = 3 cm, length = 6 cm) and a piece of titanium wire mesh (width = 5 cm, length = 6 cm), respectively. The whole reactor was tightly sealed using epoxy to maintain an anaerobic condition. Carbon dioxide that was generated by bioelectrochemical degradation of crude oil was passively collected in the headspace (50 mL) of the anode chamber, which was connected to a gas bag (Cali-5-Bond, Calibrated Instruments Inc.). The CO₂ concentration was continuously monitored using a solid-state infrared CO₂ transmitter (model GMT-221, Vaisala). The BESs were operated in three-electrode mode. The anode served as the working electrode and was poised at a potential of 0.3 V (vs Ag/AgCl reference electrode) by a potentiostat (Model: VMP-3, Bio-Logic SAS Inc., France). The cathode and an Ag/AgCl electrode (BASi RE-5B, 0.21 V vs normal hydrogen electrode (NHE) served as the counter and reference electrode, respectively. The control reactors with the same electrodes and soil samples were operated under open circuit. All experiments were conducted at room temperature (22 ± 2 °C).

Elemental Analysis, GC-FID, and GC × GC-TOF MS.

TPH measurements were conducted on days 0, 95, and 137 in active and control reactors. TPH extraction was performed according to previous studies,^{21,26} and TPH was analyzed by following the modified EPA Method 8015D and Massachusetts EPH using gas chromatography with a flame ionization detector (GC-FID). Comprehensive two-dimensional gas chromatography (coupled to a time-of-flight mass spectrometer, GC × GC-TOF MS) and elemental analysis, and carbon balances were performed on the soil samples. The details about analysis can be found in the Supporting Information (SI).

Chemical and Electrochemical Analysis. All soil analysis results were reported on a soil dry-weight basis. Soil conductivity and pH were measured at the beginning and end of the experiment in a 1:5 (w/v) soil:deionized water mixture. Soil particle size distribution was evaluated by a standard method described by Kettler et al.²⁷ Available nitrate, ammonia nitrogen, phosphate, and sulfate in soil were extracted according to Mussa et al.,²⁸ and determined according to standard methods.²⁹ Total organic carbon (TOC) in soil was performed using Walkley-Black methods. The current (*I*) was recorded and converted to current density (mA/m³) based on the working volume of the anode chamber (250 mL). The total Coulombic output (*Q*, C) was calculated as $Q = \int_0^T I dt$.

Crude Oil Extraction from Contaminated Soil. Crude oil was extracted from the soil by Soxhlet extraction. Briefly, 10 g of dried soil samples and 10 g anhydrous Na₂SO₄ were packed into 30 mm × 100 mm cellulose extraction thimble with glass wool and loaded into Soxhlet extractor. 90:10 Toluene:MeOH refluxed for 6 h with constant stirring (~40 °C).¹⁰ Solvent was evaporated under nitrogen gas, and the extracts were weighed. All solvents used in this study were HPLC grade (Sigma-Aldrich, St. Louis, MO, US).

Modified Aminopropyl Silica (MAPS) Naphthenic (NAP) Acid Extraction. Under aqueous electrospray conditions, not all acids ionize with equal ionization efficiency.³⁰ To characterize the high-molecular-weight NAP acids, the initial and final samples were further separated using

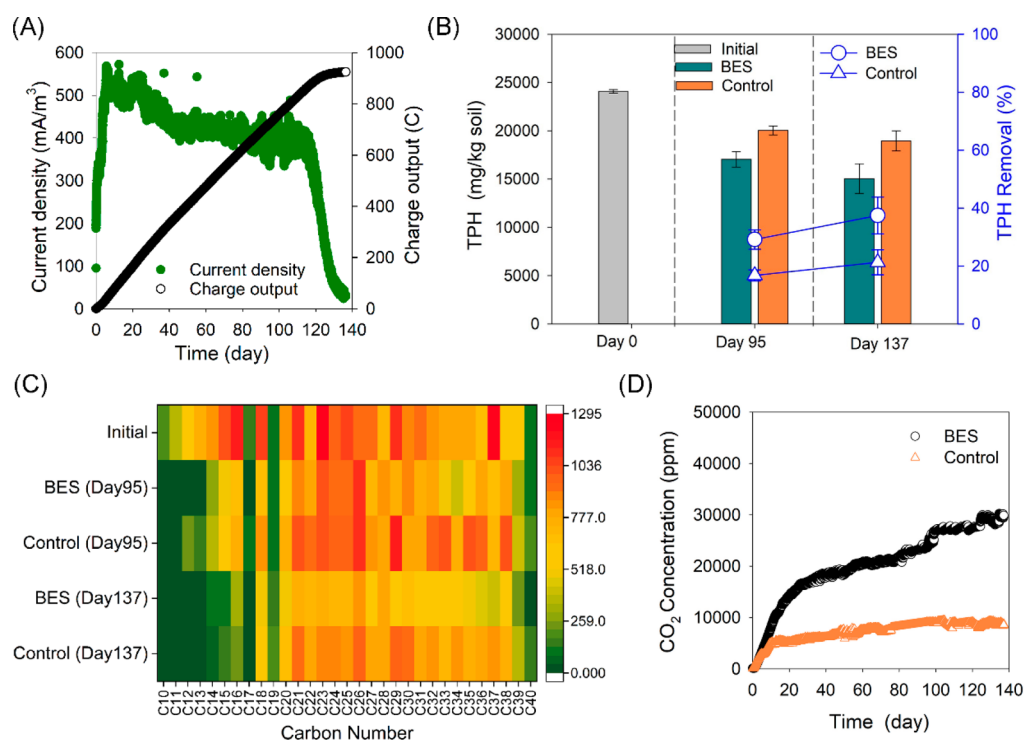


Figure 1. (A) Profile of current density and charge output in BES. (B) Total petroleum hydrocarbon (TPH) removal in BES and control. All data were means of triplicates. (C) Concentration variations of hydrocarbons with carbon number ranged from C₁₀ to C₄₀ in samples from initial soil, BES, and Control. The vertical axis indicates the different sampling times and the horizontal axis indicates the hydrocarbons with different carbon number. The color scale bar represents the hydrocarbons concentration. (D) CO₂ concentration in the headspace of the anode chamber of BES and Control. Control reactors have the same configuration as active BES reactors but were operated under open circuit.

a modified aminopropyl silica (MAPS) fractionation method,⁷ which separates NAP acids into nine fractions (MA1–MA9, MA denote MAPS fractions) corresponding to different molecular weight ranges. The details of NAP acid fractionation were described in the SI.

FT-ICR MS Analysis. Ultra-high-resolution FT-ICR MS with a custom-built 9.4 T and 21 T was performed at the National High Magnetic Field Laboratory in Tallahassee, FL.^{31,32} Crude oil extracts were diluted at a final concentration of 500 μg/mL in 50:50 (v/v) toluene:methanol with 0.125% tetramethylammonium hydroxide (TMAH) for negative-ion electrospray ionization (−) ESI FT-ICR MS at 9.4 T³³ or 4% formic acid for positive-ion electrospray ionization (+) ESI FT-ICR MS at 9.4 T.³⁴ In addition, positive-ion atmospheric pressure photoionization (+) APPI FT-ICR MS at 9.4 T was also applied to target nonpolar compounds. Samples were diluted to 250 μg/mL in toluene prior to APPI analysis.³⁵ MA1–MA9 derived from the samples were also applied to the (−) ESI FT-ICR-MS at 21 T after the separation of NAP acids. Data collection was facilitated by a modular ICR data acquisition system (PREDATOR).³⁶ Multiple individual time-domain transients were coadded, half-Hanning-apodized, zero-filled, and fast Fourier transformed prior to frequency conversion to a mass-to-charge ratio to obtain the final mass spectrum in absorption mode.³⁷ The details for mass calibration and data analysis can be found in the SI.

RESULTS AND DISCUSSION

BES Enhanced Crude Oil Degradation Measured by GC-FID. The reactor performance in terms of crude oil degradation, current, and CO₂ production was compared between the active BES reactors and control reactors. Figure

1A shows the profile of current output in an active BES reactor. The current quickly increased in the first few days until reaching a maximum current density of 569 ± 2 mA/cm² on day 5. It then gradually declined to 322 ± 6 mA/cm² on day 117. After that, it dropped rapidly, presumably due to the limited supply of biodegradable hydrocarbons or other nutrients. The accumulated charge output increased continuously over time, and its trend was consistent with the increase of carbon dioxide in BES (Figure 1A and D), indicating a bioelectrochemical conversion of contaminants to the CO₂.

Figure 1B shows the TPH degradation in active and control reactors. By day 95, TPH decreased from the initial average of 24,085 mg/kg to 17,059 mg/kg in active reactors, representing a removal of $29.2 \pm 3.4\%$. This is 1.8 times higher than that of control reactors ($16.8 \pm 2\%$). On day 137, removals of TPH were $37.5 \pm 6.3\%$ and $21.3 \pm 4.3\%$ in BES and control. BES enhanced the removal by 76% compared to the control, which should primarily be credited to the electrical circuit that channeled the electrons out and the syntrophy between electroactive microbes on the anode and hydrocarbon-degrading microorganisms in the soil.¹⁹ The time-course of degradation of *n*-alkanes (C₁₀–C₄₀) was investigated by a heat map (Figure 1C). On days 95 and 137, the overall *n*-alkane removal was 27–45% in BES and 11–27% in control. Low-molecular-weight (C₁₀–C₂₀) alkanes showed higher removal, which was 60–75% in BES and 44–73% in control. Regarding high-molecular-weight (C₂₁–C₄₀) molecules, approximately 15% (day 95) and 32% (day 137) were degraded in BES compared to ~8% in control. Degradation of *n*-alkanes in the control reactor was a natural attenuation process, which was more likely to occur as a joint achievement of anaerobic hydrocarbon-degrading microorganisms, sulfate-reducing or

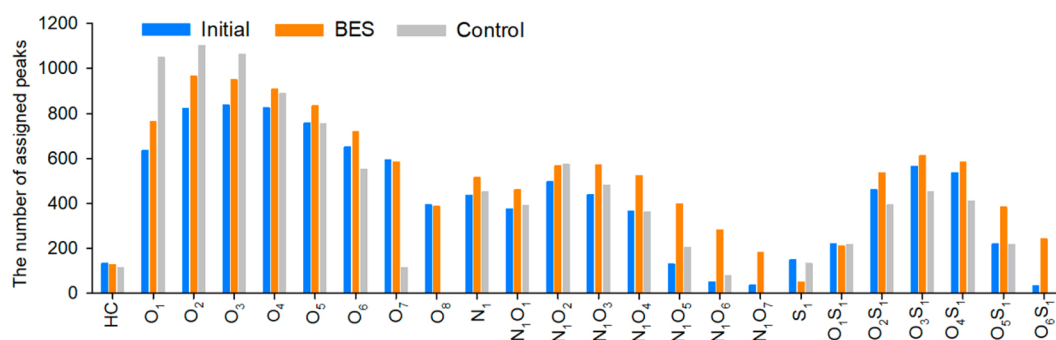


Figure 2. Heteroatom class distribution of major species based on the number of assigned peaks derived from negative-ion ESI FT-ICR mass spectra (at 9.4 T) of soil extracts from initial samples, BES, and Control.

denitrifying bacteria using sulfate, nitrate, or iron(III) as electron acceptors.^{38,39} In addition to the anaerobic hydrocarbon oxidation pathways like the fumarate addition pathway or carboxylation pathway, enhanced bioelectrochemical degradation was consistent with previous findings, as electroactive bacteria were able to respire the anode as the electron acceptor, and therefore enabled higher TPH degradation.^{19,40}

CO₂ as the Final Metabolic Product. To evaluate the oxidation level of crude oil and metabolic products, CO₂ production was monitored in real-time (Figure 1D). Both BESs and control reactors showed gradual CO₂ production with the fast rate observed in the first 10 days. This is correlated with BES current generation and believed to be due to the consumption of easily biodegradable compounds in the crude oil. After that, CO₂ concentration continued to increase in BES reactors, but the CO₂ increase in control reactors was much slower. By the end of 137 days, the CO₂ concentration in BES was 238% higher than that in the control, confirming the higher conversion of hydrocarbons in the BES reactors. This observation is in agreement with previous reports that toluene could be completely oxidized to CO₂ in a microbial fuel cell by pure culture *Geobacter metallireducens*, while no CO₂ generation was observed in the no-electrode control.²⁵ Despite the complexity of carbon characterization for crude oil, in order to quantify the carbon conversion during BES remediation, carbon balances were attempted within the BES and control reactors by comparing the initial carbon and the carbon distribution on day 137. The fractions of organic carbon derived from soil TPH and non-TPH organics in soil, electrode biomass, and CO₂ were determined and combined for the total carbon balance (Figure S2). The results showed that TPH accounted for approximately 26% of the total organic carbon (TOC) in the initial soil, and it decreased to approximately 15% in BES and 20% in the control, respectively. More TPH was converted to the CO₂ and electrode biomass in BES than the control.

GC × GC-TOF MS Analysis for Intermediate Metabolites. GC detection is limited to compounds with volatility below ~400 °C,^{11,41} and thus TPH-based characterization methods yield limited information on the chemical compositions of daughter products. We also employed GC × GC-TOF MS to identify the volatile components of parent and daughter oil extracts for obtaining molecular-level detection of intermediary metabolites. Initial and final samples were prepared, and the results were shown in Figure S3. The lower band consists of alkanes, alkenes, and cyclic alkanes according to previous reports.^{42–44} There were no obvious degradation intermediates such as alcohols, ketones, and

carboxylic acids⁴⁵ in the BES sample, indicating that these lower-molecular-weight oxygenated hydrocarbons may be generated but then consumed by microorganisms during degradation. Due to the anaerobic nature and limited soil sample availability, we were not able to obtain samples in the middle of the experiment. Residual hydrocarbons measured by GC × GC-TOF MS after BES biodegradation were highly insoluble and nonvolatile, and demonstrated structural complexity such as paraffins (Figure S3b), saturated hydrocarbon biomarkers, such as steranes (Figure S3c) and hopanes (Figure S3d), and multiring PAH chrysene (Figure S3e). Although BES is known to effectively accelerate the biodegradation of hydrocarbons, the metabolites after BES degradation are not significantly different from bioremediation. This indicates that the molecular selectivity of the microorganisms is similar, and the accumulation on biorefractory compounds would need further remediation when needed.

Because GC × GC-TOF MS can only analyze low- and mid-boiling (up to 500 °C) fractions, this technique was not able to distinguish the products of more polar, high-molecular-weight “heavy ends” (high-boiling species). Because electrospray ionization generates ions without volatility limitations, coupling ESI to FT-ICR MS can access high-molecular-weight, polar compounds that are not detectable by GC × GC. Therefore, we employed ultra-high-resolution FT-ICR MS to identify polar metabolites of petroleum bioelectrochemical degradation.

Characterization of Heteroatomic Compounds by FT-ICR MS. One interesting finding during sample elemental analysis was the change of the weight percentage of carbon, hydrogen, nitrogen, oxygen, and sulfur over time (Table S2). The greatest change of bulk compositions came from oxygen, which more than doubled in BES (3.7 wt %) compared to the initial soil (1.1 wt %). Sulfur content increased from 0.3 to 0.5 wt % in the sample after 137 days, while nitrogen remained constant (0.3 wt %). This opens a door to gain insight into the product distributions using FT-ICR MS.

Negative-ion electrospray ionization selectively ionizes acidic species (e.g., carboxylic acids and pyrrolic nitrogen) combined with FT-ICR mass spectrometry, providing elemental composition assignments to polar compounds in crude oil^{10,46} (Figure S4). Speciation by positive-ion ESI and positive-ion APPI, which target basic functionalities (e.g., pyridinic nitrogen) and nonpolar compounds (e.g., hydrocarbon), respectively, are provided in the SI Figure S5 and S6. However, as previously mentioned here, we focused on the characterization of oxygen transformation products by (–) ESI FT-ICR MS.

Molecular Weight Distribution. Figure S7 shows broadband (–) ESI FT-ICR mass spectra for the crude oil contaminated soil extracts from the initial sample, as well as final samples from active BES reactors and control reactors. Broadband spectra of these samples span a similar molecular weight range ($\sim m/z$ 250–900). The number of assigned peaks (each with signal magnitude higher than at least 6 standard deviations (σ) baseline rms noise) had a 41% increase in the BES final sample (23,930) relative to the initial sample (16,945), while an increase of 57% was observed in the control (26,570). Since compositional diversity corresponds to the number of mass spectral peaks, the first impression seems to be that more transformation products were newly generated through natural attenuation than BES. However, it is more likely that some products were more effectively degraded to CO_2 in BES that led to this observation, which was partially supported by the high TPH degradation, higher CO_2 production, and heteroatomic compounds distribution of the BES reactors.

Variation in Distribution of Total Heteroatomic Compounds after Remediation. Figure 2 depicts the distribution of heteroatom class species with the number of peaks assigned from the initial, final BES, and control samples. Compounds containing O_3 and O_2 correspond to carboxylic acids by (–) ESI comprising the highest number of peaks assigned in the initial sample, followed by O_4 , O_5 , O_6 , and O_1 classes. After biodegradation, all of the peaks in the O_1 – O_5 classes increased, suggesting that some hydrocarbon species were converted to oxygen-containing species. The bulk elemental analysis also confirmed this result: the percent of oxygen composition was more than doubled after BES biodegradation, indicating that more oxygen-containing compounds (i.e., alcohols, phenolic, ketones, aldehydes, and carboxylic acids intermediates) were produced. These results were consistent with the variation of soil pH and conductivity (Figure S8). At the end of remediation, soil pH in both BES and control decreased compared to the initial soil, but lower pH was observed in BES reactors than the control. This supports the findings that more organic acids were generated during BES remediation. Correspondingly, slightly higher conductivity was observed in BES reactors than in controls, as the conversion of nonconductive hydrocarbons to conductive organic acids led to the increase of the soil conductivity.

More interestingly, higher-order oxygenated compounds (O_4 – O_6) increased more in BES compared to those in the control, but less increase was observed in lower-order oxygenated species (O_1 – O_3). In fact, since much higher TPH biodegradation and CO_2 production were observed in BES relative to the control, there should have been more O_1 – O_3 species (e.g., alcohols, phenolic compounds, carboxylic acids) generated, but very likely they were subsequently consumed by the microbial consortia in BES to produce CO_2 as compared with more accumulation in control reactors. O_7 and O_8 had little change in the initial and final BES samples, which indicated that highly oxygenated compounds were relatively resistant to biodegradation.

Figure 3 demonstrates isoabundance-contoured plots of double bond equivalents (DBE, number of rings plus double bonds) versus carbon number for oxygenated species (O_1 – O_4) derived from (–) ESI FT-ICR MS. There were no distinct changes in the molecular distributions of oxygenated species O_1 – O_4 . DBE of oxygenated species O_1 – O_3 had slight

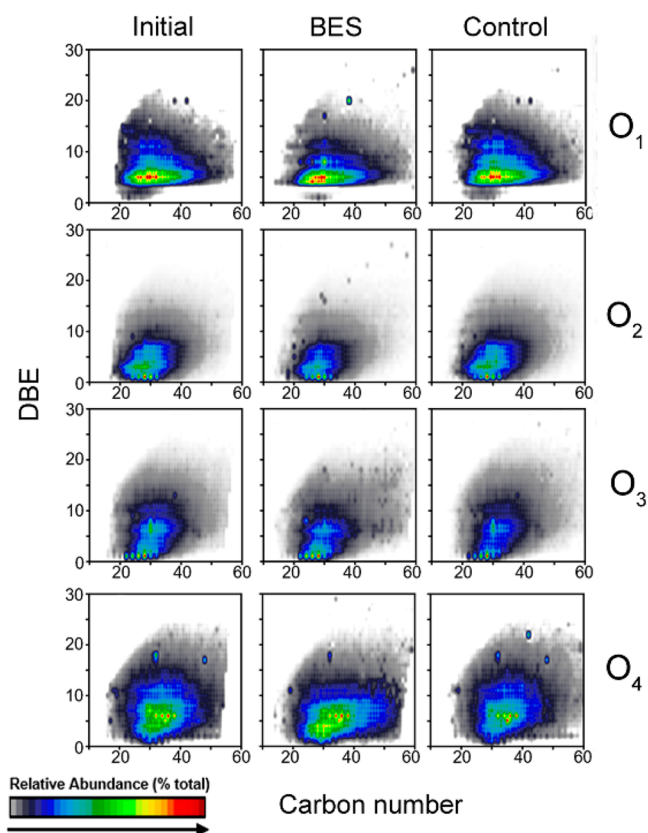


Figure 3. Negative-ion ESI-derived isoabundance-contoured plots (at 9.4 T) of double-bond equivalents (DBE) vs carbon number for the O_1 – O_4 classes for soil extracts from initial samples, BES, and Control. Each compositional image is normalized to the most abundant species within that heteroatom class for each mass spectrum.

decreases, indicating lower aromaticity after biodegradation. It should be acknowledged that not all oxygenated transformation products could be detected due to the limitations in the recovery rate and derivative efficiency. For example, the relative abundance of high-molecular-weight oxygen-containing compounds was relatively low due to less ionization efficiency. For this reason, it may not be accurate to compare and characterize oxygen transformation products side-by-side due to different ionization efficiencies among samples. Therefore, we also isolated and fractionated oxygen transformation products, like NAP acids, into different molecular weight ranges by grouping NAP acids into fractions with a similar ionization efficiency for direct comparison.

Naphthenic (NAP) Acid Extraction and Characterization by Modified Aminopropyl Silica (MAPS). In Figure S4, the highest relative abundance of heteroatoms is in the O_2 class, which is related to compounds of the NAP acids, and needs to be further investigated. Isolation and fractionation of crude oil compounds on the MAPS method have been reported to identify the chemical functionality of NAP acids.^{7,47} To better understand and compare the variation of acidic functional groups before and after BES biodegradation, the samples were further separated into fractions MA1–MA9 by MAPS extraction. The percent composition of acidic oxygen compounds by MAPS is shown in Figure S9. The total percent of recoveries were 91.8% and 87.0% for the initial and final samples, respectively. The major compounds were nonacidic compounds eluting with dichloromethane (DCM),

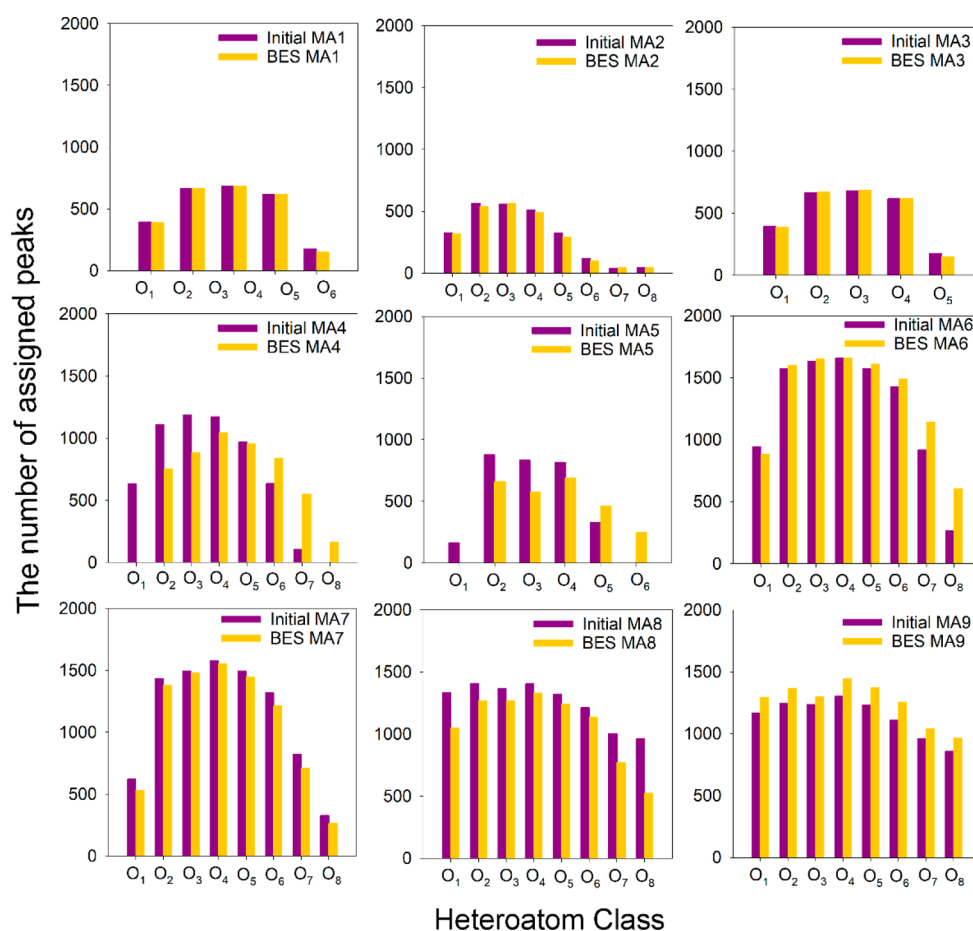


Figure 4. Heteroatom class distribution for oxygen-containing compounds isolated into discrete fractions (MA1–MA9) by modified aminopropyl silica (MAPS) derived from negative-ion 21 T ESI FT-ICR mass spectra of soil extracts from initial samples and BES.

which counted around 79.4% of the initial sample and 68.5% of the final BES sample (Figure S9). After bioelectrochemical degradation, the total acids increased by nearly 48%, from 12.4% to 18.4%. MA4 had the highest content in all MAPS fractions, accounting for 38% and 47% of the total acids in the initial and final samples, respectively. The most notable changes were observed in fractions MA5 and MA7, which had a maximum increase of ~ 7 -fold and 9-fold, respectively, after BES degradation, suggesting that the newly generated daughter products were likely high-molecular-weight acidic species. Other MAPS fractions showed minimal changes in percentage mass recovery between the initial and final samples.

The (–) ESI FT-ICR mass spectra for all fractions, MA1–MA9, of the initial sample are shown in Figure S10. There were approximately 175,000 assignments for fractions MA1–MA9, which is more than 9-fold that of the initial spectrum before fractionation ($\sim 17,000$ assigned peaks in Figure S7). High-molecular-weight acids in MPAS fractions exhibited a higher number of assigned peaks. For example, MA6, MA7, MA8, and MA9 fractions had 33,177, 24,877, 41,699, and 34,206 assigned peaks, respectively. These high-molecular-weight fractions also extended the characterization of the isolated initial sample to ~ 1000 Da. These results demonstrate that high-molecular-weight NAP acids existing in the initial sample are suppressed by low-molecular-weight NAP acids, that are preferentially ionized with high efficiency.⁷ Therefore, it is necessary to isolate acidic species, especially high-

molecular-weight acids, before chemical functionality of NAP acids can be identified.

Heteroatom Class Compositions of Different Fractions of NAP Acids. The (–) ESI-derived heteroatom oxygen-containing compounds (O_1 – O_6) distribution of all isolated fractions MA1–MA9 is shown in Figure S11. In both initial and final BES samples, each fraction in MA1–MA9 presented a similar distribution of oxygenated species, and O_2 acids were the most abundant heteroatom class. Although isolating NAP acids into nine fractions based on molecular weight aimed to obtain similar ionization efficiency for each fraction, O_2 species exhibited higher relative abundance, presumably due to higher ionization efficiency for O_2 compounds using (–) ESI compared to other oxygenated species. Thus, to better compare acidic fractions between initial and final samples, the oxygen-containing compounds distribution of all isolated fractions MA1–MA9 based on the number of assigned peaks rather than relative abundance (Figure 4). Note that MA4 and MA5 fractions in BES have a remarkable decrease in lower-order NAP acids (O_1 – O_4) and a concurrent increase in higher-order NAP acids (O_5 – O_8), indicating that lower-order NAP acids are further transformed into highly polar NAP acids, such as multi-ring dicarboxylic acids.¹⁰

Identification of Acidic Transformation Products. To further illustrate acidic compositional variation after BES degradation, iso-abundance plots that present DBE versus carbon number were constructed for heteroatomic oxygen-

containing compounds (O_1 – O_6) in MA1–MA9 fractions (Figure S12). For easier comparison, we select the three MAPS fractions of MA4, MA5, and MA7 that have changed the most in the initial and BES samples, as shown in Figure 5. Relative-

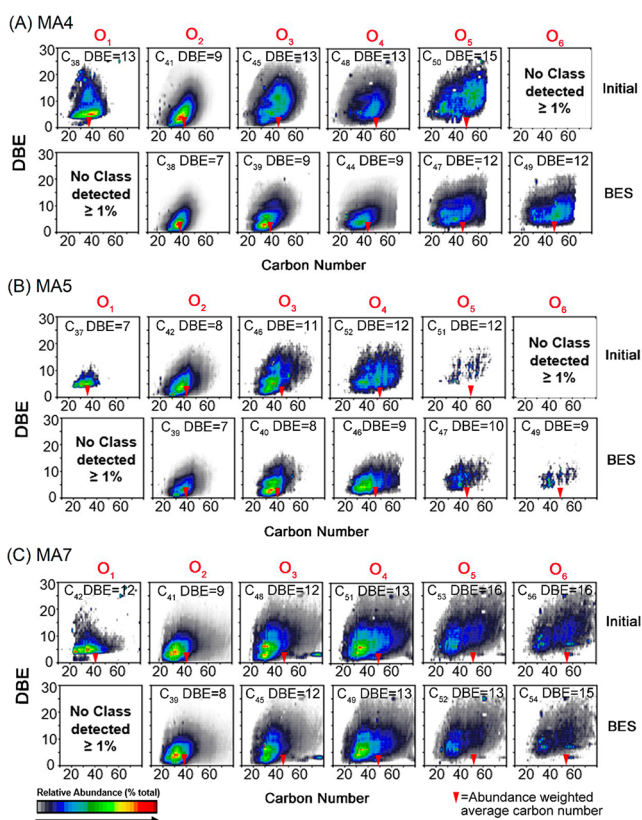


Figure 5. Isoabundance color-coded contour plots of double-bond equivalents (DBE) vs carbon number for the O_1 – O_6 classes of the three selected MAPS fractions derived from negative-ion ESI FT-ICR MS at 21 T: (A) MA4, (B) MA5, and (C) MA7 for soil extracts from initial samples and BESs. Relative-abundance-weighted average DBE and carbon number are shown as red arrows in each image. For variations of all nine fractions (MA1–MA9), please refer to Figure S12.

abundance-weighted average DBE and carbon number are also shown in each image. Overall, for the O_1 – O_6 classes, the increase in abundance-weighted average carbon number was correlated with the increase in molecular weight. This is represented from $\sim C_{30}$ for fractions MA1–MA3 to $\sim C_{60}$ for fractions MA6–MA9.

For the O_1 class, fractions MA1–MA9 exhibited a slightly bimodal DBE distribution, indicative of alcohols (DBE = 1) and alkylphenol compounds (DBE = 4–5).⁶ However, when comparing O_1 class in each fraction between initial and final samples, we found that O_1 species from MA4 and MA5 became absent in the final BES sample. This shift occurs concurrent with an increase in O_5 – O_6 species in BES, which suggests the oxidation of O_1 intermediates to form one or more carboxylic acids did not occur in the parent oil extract, as observed in other biodegraded weathered oil studies.¹⁰

For the O_2 class in the initial sample, although the carbon number increased along with successive elution fractions from MA1 to MA9, the most abundant DBE remained approximately the same (DBE = 2–7). This suggests that monocyclic or multiple-ring NAP acids were kept the same.⁴⁸ Additionally,

fractions MA5 and MA6 span a bimodal distribution, with another typical fatty acid structure at DBE 1 with C_{30} , which is related to *n*-alkane biodegradation via β -oxidation pathway.⁴⁹ A similar trend was observed in the BES final sample. Furthermore, low-molecular-weight fractions MA1–MA3 in O_1 and O_2 classes closed to the planar stability limit across a narrow carbon number range up to $\sim C_{30}$, that correspond to condensed aromatic structures.⁵⁰

For the O_3 class, clear bimodality was observed in MA2 and MA3, suggesting the presence of at least two different core structures in the acids. It was predominately DBE = 3–10 and 12–14 across a similar carbon number range (C_{30} – C_{35}), indicative of a carboxylic acid group with an additional ring and/or double bond(s) structure from degradation of aromatic hydrocarbons, or carboxylic acid group with a single hydroxyl group (e.g., hydroxycarboxylic acids) structure formed from hydroxylated parent NAP acids.^{12,51} MA4 and MA5 fractions in the O_3 class displayed a decrease in both DBE and carbon number range after BES degradation, and other fractions in O_3 revealed little changes between the initial and final samples. Similarly, compounds of MA4 and MA5 in O_4 class, most likely dicarboxylic acids, showed a decrease in relative abundance weight-average carbon number and DBE in the final BES sample. Furthermore, MA7–MA9 exhibited a bimodal DBE distribution for the O_4 class, indicating two possible stable core structures corresponding to dicarboxylic acids or carboxylic acids with two hydroxyl groups.

Bioelectrochemical Oxygenated Daughter Products.

The negative-ion ESI FT-ICR MS revealed the distributions of heteroatom oxygen-containing compounds, especially NAP acids, after bioelectrochemical crude oil degradation. The degradation took place in a strict oxygen-free environment, and there were no other electron acceptors such as sulfate or nitrate except the anode. The variation of oxygenated daughter products was consistent with environmental conditions. Since there was no oxygen present in the system, hydrocarbon activation may be initiated by addition of an oxygen-containing organic species like fumarate, which led to carbon elongation.^{52,53} However, due to complexity of the crude oil and intermediate products, precise carbon flux analysis was not possible in the study. Previous study did report that low-order oxygenated species were transformed into highly polar, oxygen-containing compounds (O_x , where $x > 3$), supporting a similar hypothesis.¹⁰ It is likely that once catabolism was initiated, anode reduction could facilitate β -oxidation, but further investigations are needed to test these hypotheses using more defined substrates and carbon flux analysis. After BES degradation, the amount of total acids increased, and the contributions of newly generated NAP acids were mainly from higher-order oxygen species (O_5 – O_6) with increasing hydrophobicity, indicating secondary oxidation of lower-order oxygenated species to generate acidic compounds that contain more carboxylic acids.¹⁰ Additionally, a decrease of abundant of lower-order oxygen species (O_1) revealed that *n*-alkane degraded via β -oxidation to the lower-weight oxygenated daughter products, such as *n*-alcohols in O_1 class, and subsequently transformed to *n*-fatty acids in O_2 class, which can be further oxidized by EAB to produce CO_2 .

Future Work. This study shed light on daughter product distribution after bioelectrochemical crude oil degradation, and it revealed the changes in oxygenated compounds. However, only initial and final samples were able to be obtained for analyses; therefore, the results did not reflect the production

and consumption cycles of heteroatom Ox class compounds, like carboxylic acids during degradation. To completely elucidate degradation mechanisms of hydrocarbons, further studies can use staged sampling and present the variations of intermediate transformation products over time, which will require a careful sampling process and a significant amount of crude oil samples and analytical budget. In addition, transformation products combined with microbial community structure and function need to be further investigated to understand microbial ecological interactions on the degradation of recalcitrant hydrocarbons. It would also be desired to characterize sulfur- and nitrogen-containing metabolites.^{54–56} Deciphering the degradation pathways and products is important for further technology deployment and regulatory review and approval.

■ ASSOCIATED CONTENT

SI Supporting Information

The Supporting Information is available free of charge at <https://pubs.acs.org/doi/10.1021/acs.est.9b06164>.

Details on experimental methods; images on reactors setup (Figure S1); carbon balance analysis (Figure S2); GC × GC-TOF MS analysis (Figure S3); additional results on ESI FT-ICR MS analysis (Figures S4–S7); pH and conductivity profiles (Figure S8); detailed MAPS fractions analyses (Figures S9–S13); initial soil sample characterizations (Tables S1–S2) (PDF)

■ AUTHOR INFORMATION

Corresponding Author

Zhiyong Jason Ren – Department of Civil and Environmental Engineering and the Andlinger Center for Energy and the Environment, Princeton University, Princeton, New Jersey 08544, United States; Department of Civil, Environmental and Architectural Engineering, University of Colorado Boulder, Boulder, Colorado 80309, United States; orcid.org/0000-0001-7606-0331; Email: zjren@princeton.edu

Authors

Huan Wang – Department of Civil and Environmental Engineering and the Andlinger Center for Energy and the Environment, Princeton University, Princeton, New Jersey 08544, United States; Department of Civil, Environmental and Architectural Engineering, University of Colorado Boulder, Boulder, Colorado 80309, United States

Lu Lu – Department of Civil and Environmental Engineering and the Andlinger Center for Energy and the Environment, Princeton University, Princeton, New Jersey 08544, United States

Huan Chen – National High Magnetic Field Laboratory, Florida State University, Tallahassee, Florida 32310, United States

Amy M. McKenna – National High Magnetic Field Laboratory, Florida State University, Tallahassee, Florida 32310, United States; orcid.org/0000-0001-7213-521X

Jie Lu – National High Magnetic Field Laboratory, Florida State University, Tallahassee, Florida 32310, United States

Song Jin – Advanced Environmental Technologies, LLC, Fort Collins, Colorado 80525, United States

Yi Zuo – Chevron Energy Technology Company, San Ramon, California 94583, United States

Fernando L. Rosario-Ortiz – Department of Civil, Environmental and Architectural Engineering, University of Colorado Boulder, Boulder, Colorado 80309, United States; orcid.org/0000-0002-3311-9089

Complete contact information is available at: <https://pubs.acs.org/doi/10.1021/acs.est.9b06164>

Notes

The authors declare no competing financial interest.

■ ACKNOWLEDGMENTS

This work was supported by the Chevron Energy Technology Company. We appreciate feedback from Chevron and the reviewers. FT-ICR part was performed at the National High Magnetic Field Laboratory Ion Cyclotron Resonance user facility, which was supported by the National Science Foundation Division of Chemistry through DMR-164479, and the State of Florida.

■ REFERENCES

- (1) Altgelt, K. H. *Composition and analysis of heavy petroleum fractions*; CRC Press: 1993.
- (2) Widdel, F.; Rabus, R. Anaerobic biodegradation of saturated and aromatic hydrocarbons. *Curr. Opin. Biotechnol.* **2001**, *12* (3), 259–276.
- (3) Focht, J. Anaerobic biodegradation of aromatic hydrocarbons: pathways and prospects. *J. Mol. Microbiol. Biotechnol.* **2008**, *15* (2–3), 93–120.
- (4) Haritash, A.; Kaushik, C. Biodegradation aspects of polycyclic aromatic hydrocarbons (PAHs): a review. *J. Hazard. Mater.* **2009**, *169* (1–3), 1–15.
- (5) Leahy, J. G.; Colwell, R. R. Microbial degradation of hydrocarbons in the environment. *Microbiol. Rev.* **1990**, *54* (3), 305–315.
- (6) Liao, Y.; Shi, Q.; Hsu, C. S.; Pan, Y.; Zhang, Y. Distribution of acids and nitrogen-containing compounds in biodegraded oils of the Liaohe Basin by negative ion ESI FT-ICR MS. *Org. Geochem.* **2012**, *47*, 51–65.
- (7) Rowland, S. M.; Robbins, W. K.; Corilo, Y. E.; Marshall, A. G.; Rodgers, R. P. Solid-phase extraction fractionation to extend the characterization of naphthenic acids in crude oil by electrospray ionization Fourier transform ion cyclotron resonance mass spectrometry. *Energy Fuels* **2014**, *28* (8), 5043–5048.
- (8) Kim, S.; Stanford, L. A.; Rodgers, R. P.; Marshall, A. G.; Walters, C. C.; Qian, K.; Wenger, L. M.; Mankiewicz, P. Microbial alteration of the acidic and neutral polar NSO compounds revealed by Fourier transform ion cyclotron resonance mass spectrometry. *Org. Geochem.* **2005**, *36* (8), 1117–1134.
- (9) Mohler, R. E.; O'Reilly, K. T.; Zemo, D. A.; Tiwary, A. K.; Magaw, R. I.; Synowiec, K. A. Non-targeted analysis of petroleum metabolites in groundwater using GC×GC-TOFMS. *Environ. Sci. Technol.* **2013**, *47* (18), 10471–10476.
- (10) Chen, H.; Hou, A. X.; Corilo, Y. E.; Lin, Q. X.; Lu, J.; Mendelsohn, I. K.; Zhang, R.; Rodgers, R. P.; McKenna, A. M. 4 Years after the Deepwater Horizon Spill: Molecular Transformation of Macondo Well Oil in Louisiana Salt Marsh Sediments Revealed by FT-ICR Mass Spectrometry. *Environ. Sci. Technol.* **2016**, *50* (17), 9061–9069.
- (11) McKenna, A. M.; Nelson, R. K.; Reddy, C. M.; Savory, J. J.; Kaiser, N. K.; Fitzsimmons, J. E.; Marshall, A. G.; Rodgers, R. P. Expansion of the analytical window for oil spill characterization by ultrahigh resolution mass spectrometry: Beyond gas chromatography. *Environ. Sci. Technol.* **2013**, *47* (13), 7530–7539.
- (12) Pan, Y.; Liao, Y.; Shi, Q. Variations of Acidic Compounds in Crude Oil during Simulated Aerobic Biodegradation: Monitored by

Semiquantitative Negative-Ion ESI FT-ICR MS. *Energy Fuels* **2017**, *31* (2), 1126–1135.

(13) Lim, M. W.; Von Lau, E.; Poh, P. E. A comprehensive guide of remediation technologies for oil contaminated soil—present works and future directions. *Mar. Pollut. Bull.* **2016**, *109* (1), 14–45.

(14) Lovley, D. R. Anaerobic benzene degradation. *Biodegradation* **2000**, *11* (2–3), 107–116.

(15) Xu, R.; Obbard, J. P. Biodegradation of polycyclic aromatic hydrocarbons in oil-contaminated beach sediments treated with nutrient amendments. *J. Environ. Qual.* **2004**, *33* (3), 861–867.

(16) Wang, H.; Luo, H.; Fallgren, P.; Jin, S.; Ren, Z. J. Bioelectrochemical Platform for Sustainable Environmental Remediation and Energy Generation. *Biotechnol. Adv.* **2015**, *33* (3–4), 317–334.

(17) Morris, J. M.; Jin, S.; Crimi, B.; Pruden, A. Microbial fuel cell in enhancing anaerobic biodegradation of diesel. *Chem. Eng. J.* **2009**, *146* (2), 161–167.

(18) Wang, X.; Cai, Z.; Zhou, Q.; Zhang, Z.; Chen, C. Bioelectrochemical stimulation of petroleum hydrocarbon degradation in saline soil using U-tube microbial fuel cells. *Biotechnol. Bioeng.* **2012**, *109* (2), 426–433.

(19) Wang, H.; Lu, L.; Mao, D.; Huang, Z.; Cui, Y.; Jin, S.; Zuo, Y.; Ren, Z. J. Dominance of electroactive microbiomes in bioelectrochemical remediation of hydrocarbon-contaminated soils with different textures. *Chemosphere* **2019**, *235*, 776–784.

(20) Logan, B. E.; Hamelers, B.; Rozendal, R.; Schröder, U.; Keller, J.; Freguia, S.; Aelterman, P.; Verstraete, W.; Rabaey, K. Microbial fuel cells: methodology and technology. *Environ. Sci. Technol.* **2006**, *40* (17), 5181–5192.

(21) Lu, L.; Yazdi, H.; Jin, S.; Zuo, Y.; Fallgren, P. H.; Ren, Z. J. Enhanced bioremediation of hydrocarbon-contaminated soil using pilot-scale bioelectrochemical systems. *J. Hazard. Mater.* **2014**, *274*, 8–15.

(22) Li, T.; Wang, X.; Zhou, Q.; Liao, C.; Zhou, L.; Wan, L.; An, J.; Du, Q.; Li, N.; Ren, Z. J. Swift acid rain sensing by synergistic rhizospheric bioelectrochemical responses. *ACS Sens.* **2018**, *3* (7), 1424–1430.

(23) Li, X.; Wang, X.; Ren, Z. J.; Zhang, X.; Li, N.; Zhou, Q. Sand Amendment Enhances Bioelectrochemical Remediation of Petroleum Hydrocarbon Contaminated Soil. *Chemosphere* **2015**, *141*, 62–70.

(24) Daghighi, M.; Aulenta, F.; Vaiopoulou, E.; Franzetti, A.; Arends, J. B.; Sherry, A.; Suárez-Suárez, A.; Head, I. M.; Bestetti, G.; Rabaey, K. Electrobioremediation of oil spills. *Water Res.* **2017**, *114*, 351–370.

(25) Zhang, T.; Gannon, S. M.; Nevin, K. P.; Franks, A. E.; Lovley, D. R. Stimulating the anaerobic degradation of aromatic hydrocarbons in contaminated sediments by providing an electrode as the electron acceptor. *Environ. Microbiol.* **2010**, *12* (4), 1011–1020.

(26) Lu, L.; Huggins, T.; Jin, S.; Zuo, Y.; Ren, Z. J. Microbial metabolism and community structure in response to bioelectrochemically enhanced remediation of petroleum hydrocarbon-contaminated soil. *Environ. Sci. Technol.* **2014**, *48* (7), 4021–4029.

(27) Kettler, T.; Doran, J. W.; Gilbert, T. Simplified method for soil particle-size determination to accompany soil-quality analyses. *Soil Sci. Soc. Am. J.* **2001**, *65* (3), 849–852.

(28) American Public Health Association, American Water Works Association, and Water Environment Federation. *Standard Methods for the Examination of Water and Wastewater*, 20th ed.; APHA-AWWA-WEF: Washington, DC, 1998.

(29) Liu, Q.; Ren, Z. J.; Huang, C.; Liu, B.; Ren, N.; Xing, D. Multiple syntrophic interactions drive biohydrogen production from waste sludge in microbial electrolysis cells. *Biotechnol. Biofuels* **2016**, *9* (1), 162.

(30) Hindle, R.; Noestheden, M.; Peru, K.; Headley, J. Quantitative analysis of naphthenic acids in water by liquid chromatography–accurate mass time-of-flight mass spectrometry. *J. Chromatogr. A* **2013**, *1286*, 166–174.

(31) Kaiser, N. K.; Quinn, J. P.; Blakney, G. T.; Hendrickson, C. L.; Marshall, A. G. A novel 9.4 T FTICR mass spectrometer with

improved sensitivity, mass resolution, and mass range. *J. Am. Soc. Mass Spectrom.* **2011**, *22* (8), 1343–1351.

(32) Hendrickson, C. L.; Quinn, J. P.; Kaiser, N. K.; Smith, D. F.; Blakney, G. T.; Chen, T.; Marshall, A. G.; Weisbrod, C. R.; Beu, S. C. 21 T Fourier transform ion cyclotron resonance mass spectrometer: a national resource for ultrahigh resolution mass analysis. *J. Am. Soc. Mass Spectrom.* **2015**, *26* (9), 1626–1632.

(33) Lobodin, V. V.; Juyal, P.; McKenna, A. M.; Rodgers, R. P.; Marshall, A. G. Tetramethylammonium hydroxide as a reagent for complex mixture analysis by negative ion electrospray ionization mass spectrometry. *Anal. Chem.* **2013**, *85* (16), 7803–7808.

(34) Ruddy, B. M.; Huettel, M.; Kostka, J. E.; Lobodin, V. V.; Bythell, B. J.; McKenna, A. M.; Aeppli, C.; Reddy, C. M.; Nelson, R. K.; Marshall, A. G. Targeted petroleomics: analytical investigation of Macondo well oil oxidation products from Pensacola Beach. *Energy Fuels* **2014**, *28* (6), 4043–4050.

(35) Purcell, J. M.; Rodgers, R. P.; Hendrickson, C. L.; Marshall, A. G. Speciation of nitrogen containing aromatics by atmospheric pressure photoionization or electrospray ionization Fourier transform ion cyclotron resonance mass spectrometry. *J. Am. Soc. Mass Spectrom.* **2007**, *18* (7), 1265–1273.

(36) Blakney, G. T.; Hendrickson, C. L.; Marshall, A. G. Predator data station: a fast data acquisition system for advanced FT-ICR MS experiments. *Int. J. Mass Spectrom.* **2011**, *306* (2), 246–252.

(37) Xian, F.; Hendrickson, C. L.; Blakney, G. T.; Beu, S. C.; Marshall, A. G. Automated broadband phase correction of Fourier transform ion cyclotron resonance mass spectra. *Anal. Chem.* **2010**, *82* (21), 8807–8812.

(38) da Cruz, G. F.; de Vasconcelos, S. P.; Angolini, C. F.; Dellagnezze, B. M.; Garcia, I. N.; de Oliveira, V. M.; dos Santos Neto, E. V.; Marsaioli, A. J. Could petroleum biodegradation be a joint achievement of aerobic and anaerobic microorganisms in deep sea reservoirs? *AMB Express* **2011**, *1* (1), 47.

(39) Aeppli, C.; Carmichael, C. A.; Nelson, R. K.; Lemkau, K. L.; Graham, W. M.; Redmond, M. C.; Valentine, D. L.; Reddy, C. M. Oil weathering after the Deepwater Horizon disaster led to the formation of oxygenated residues. *Environ. Sci. Technol.* **2012**, *46* (16), 8799–8807.

(40) Spormann, A. M.; Widdel, F. Metabolism of alkylbenzenes, alkanes, and other hydrocarbons in anaerobic bacteria. *Biodegradation* **2000**, *11* (2–3), 85–105.

(41) Frysinger, G. S.; Gaines, R. B.; Xu, L.; Reddy, C. M. Resolving the unresolved complex mixture in petroleum-contaminated sediments. *Environ. Sci. Technol.* **2003**, *37* (8), 1653–1662.

(42) Van De Weghe, H.; Vanermen, G.; Gemoets, J.; Lookman, R.; Bertels, D. Application of comprehensive two-dimensional gas chromatography for the assessment of oil contaminated soils. *J. Chromatogr. A* **2006**, *1137* (1), 91–100.

(43) Betancourt, S. S.; Ventura, G. T.; Pomerantz, A. E.; Vilorio, O.; Dubost, F. X.; Zuo, J.; Monson, G.; Bustamante, D.; Purcell, J. M.; Nelson, R. K. Nanoaggregates of asphaltene in a reservoir crude oil and reservoir connectivity. *Energy Fuels* **2009**, *23* (3), 1178–1188.

(44) Ventura, G. T.; Simoneit, B. R.; Nelson, R. K.; Reddy, C. M. The composition, origin and fate of complex mixtures in the maltene fractions of hydrothermal petroleum assessed by comprehensive two-dimensional gas chromatography. *Org. Geochem.* **2012**, *45*, 48–65.

(45) Mao, D.; Lookman, R.; Weghe, H. V. D.; Weltens, R.; Vanermen, G.; Brucker, N. D.; Diels, L. Combining HPLC-GC/MS, GCXGC/ToF-MS, and selected ecotoxicity assays for detailed monitoring of petroleum hydrocarbon degradation in soil and leaching water. *Environ. Sci. Technol.* **2009**, *43* (20), 7651–7657.

(46) Hughey, C. A.; Rodgers, R. P.; Marshall, A. G.; Qian, K.; Robbins, W. K. Identification of acidic NSO compounds in crude oils of different geochemical origins by negative ion electrospray Fourier transform ion cyclotron resonance mass spectrometry. *Org. Geochem.* **2002**, *33* (7), 743–759.

(47) Clingenpeel, A. C.; Rowland, S. M.; Corilo, Y. E.; Zito, P.; Rodgers, R. P. Fractionation of interfacial material reveals a

continuum of acidic species that contribute to stable emulsion formation. *Energy Fuels* **2017**, *31* (6), 5933–5939.

(48) Zhang, Y.; Shi, Q.; Li, A.; Chung, K. H.; Zhao, S.; Xu, C. Partitioning of crude oil acidic compounds into subfractions by extrography and identification of isoprenoidyl phenols and tocopherols. *Energy Fuels* **2011**, *25* (11), 5083–5089.

(49) Alvarez, H. M. Relationship between β -oxidation pathway and the hydrocarbon-degrading profile in actinomycetes bacteria. *Int. Biodeterior. Biodegrad.* **2003**, *52* (1), 35–42.

(50) McKenna, A. M.; Chacón-Patiño, M. L.; Weisbrod, C. R.; Blakney, G. T.; Rodgers, R. P. Molecular-Level Characterization of Asphaltenes Isolated from Distillation Cuts. *Energy Fuels* **2019**, *33* (3), 2018–2029.

(51) Han, X.; Scott, A. C.; Fedorak, P. M.; Bataineh, M.; Martin, J. W. Influence of molecular structure on the biodegradability of naphthenic acids. *Environ. Sci. Technol.* **2008**, *42* (4), 1290–1295.

(52) Bian, X.-Y.; Mbadinga, S. M.; Liu, Y.-F.; Yang, S.-Z.; Liu, J.-F.; Ye, R.-Q.; Gu, J.-D.; Mu, B.-Z. Insights into the anaerobic biodegradation pathway of n-alkanes in oil reservoirs by detection of signature metabolites. *Sci. Rep.* **2015**, *5*, 9801.

(53) Heider, J.; Spormann, A. M.; Beller, H. R.; Widdel, F. Anaerobic bacterial metabolism of hydrocarbons. *FEMS Microbiol. Rev.* **1998**, *22* (5), 459–473.

(54) Pan, Y.; Liao, Y.; Shi, Q.; Hsu, C. S. Acidic and neutral polar NSO compounds in heavily biodegraded oils characterized by negative-ion ESI FT-ICR MS. *Energy Fuels* **2013**, *27* (6), 2960–2973.

(55) Thauer, R. K.; Stackebrandt, E.; Hamilton, W. A. Energy metabolism and phylogenetic diversity of sulphate-reducing bacteria. In *Sulphate-Reducing Bacteria* 2007; pp 1–37.

(56) Liu, W.; Liao, Y.; Pan, Y.; Jiang, B.; Zeng, Q.; Shi, Q.; Hsu, C. S. Use of ESI FT-ICR MS to investigate molecular transformation in simulated aerobic biodegradation of a sulfur-rich crude oil. *Org. Geochem.* **2018**, *123*, 17–26.